ECS Transactions, 33 (2) 245-257 (2010)
10.1149/1.3485262 ©The Electrochemical Society

Dye-Sensitized Solar Cells Fabricated From Atomic Layer Deposited Photoanodes on Aerogel Scaffolds

David M. Hess[a], Mohammed Mushfiq[a], Rashmi Dalvi[a], Raymond Winter[a], Uma Sampathkumaran[a], Kisholoy Goswami[a], Angel Yanguas-Gil[b], Jeffrey W. Elam[b]

[a]InnoSense LLC, 2531 W. 237th Street, Ste. 127, Torrance, CA 90505, USA
[b]Argonne National Laboratory, 9700 South Cass Avenue, Argonne, IL 60439, USA

Dye-sensitized solar cells (DSSCs) based on mesoporous, high surface area nanocrystalline titania (TiO_2) exhibiting up to 11% solar energy-conversion efficiencies are promising materials for cost-effective devices. Our objective here is to realize a cost-effective fabrication technique coupled with suitable device architecture of nanostructured DSSCs to achieve high photoconversion efficiencies. Atomic layer deposition (ALD) offers an attractive synthetic route for fabricating conformal photoanode coating materials on a nanoporous scaffold. Here, we used silica aerogels processed by doctor blading as structural scaffolds on transparent conducting oxide substrates, to promote subsequent conformal growth of thin films of TiO_2 and aluminum-doped zinc oxide (AZO) by ALD. The resulting interdigitated architecture of the photoanodes can facilitate fast electron transfer. Dye sensitization of the photoanodes was accomplished using di-tetrabutylammonium cis-bis(isothiocyanato)bis(2,2'-bipyridyl-4,4'-dicarboxylate)ruthenium(II) ("N719", Dyesol, B2 dye) and assembled into photocells using liquid electrolytes. Co-sensitization with a second dye was found to increase the photon absorption and cell efficiency.

Introduction

More energy from sunlight strikes the Earth in just one hour (4.3×10^{20} J) than all the energy consumed on the planet in an entire year (4.1×10^{20} J) (1). The demand for photovoltaic (PV) devices is expected to double every 3–4 years and reach $75B in 2020 (2). In addition, the widespread application of PV as a primary means for generating electrical power would exceed these estimates by many orders of magnitude. Nearly all solar cells in the world are manufactured using crystalline silicon; monocrystalline solar cells (14–17% average efficiency) or polycrystalline solar cells (13–15% average efficiency). The manufacturing of high purity, crystalline silicon for PV devices is an expensive and extremely energy-intensive process performed at high temperatures (3,4) In addition most of the greenhouse gases and other environmental pollutants are emitted during this step. The energy required to manufacture monocrystalline silicon PVs is 5×10^9 J per square meter of PV (5). In contrast to crystalline silicon PV devices, dye-sensitized solar cells (DSSCs) are manufactured using less expensive, low-temperature processes that consume less energy (6).

DSSCs are photovoltaic devices that use a monolayer of organic dye to absorb sunlight (7). The dye is fixed to a porous layer with a thickness of 10 μm comprised of a network of nanoparticles. These nanoparticles are composed of a wide-bandgap semi-conducting material such as titanium dioxide (TiO_2). The photoexcited dye molecule injects an electron into the TiO_2 conduction band. The electron subsequently diffuses through the nanoparticle network before reaching the anode, a transparent conducting oxide (i.e., TCO) film on a glass substrate. The counter electrode is typically a platinized glass plate, which supplies holes to an electrolyte solution of iodide/triiodide in acetonitrile. The iodide/triiodide serves as the redox shuttle to reduce dye molecules and complete the electrical circuit. Despite the cost advantage of conventional DSSCs, lower efficiency compared to crystalline silicon PV has limited commercial deployment. Lower efficiency is inherent to the architecture of conventional DSSCs: each photoelectron is forced to slowly diffuse through the 10 micron thickness of the TiO_2 nanoparticle array to reach the TCO electrode where it can be collected. During this slow transit time (several milliseconds), some electrons recombine with holes in the electrolyte solution generating heat, but no electric power. This slow transit time limits the maximum usable thickness of the TiO_2 nanoparticle array to ~10 microns, and consequently conventional DSSCs cannot harvest all available sunlight. This effect limits the efficiencies of conventional DSSCs to ~11% (8)

In contrast, ANL researchers have recently demonstrated the benefits of combining ALD layers with nanoporous substrates to improve the performance of DSSCs. Record efficiencies were achieved for ZnO nanotube DSSCs (9). In addition, functioning DSSCs were created using ALD to coat aerogel thin films with ZnO and TiO_2 (10,11). They also recently developed an improved architecture for DSSCs (Figure 1[right]) that promises to increase efficiency beyond 11%. A porous, high surface area silica aerogel thin film is applied to the TCO substrate and coated with a thin layer of TCO material using ALD. Next, a thin, 10 nm layer of TiO_2 is applied by ALD over the TCO layer. In other words, the TCO layer is "interdigitated" with the TiO_2 semiconducting layer. The electrode structure is annealed to produce anatase, the crystalline phase of the ALD TiO_2 which is optimal for the DSSCs. The remainder of the PV is fabricated using standard DSSC procedures. In the nanostructured DSSC, the photoelectron in the TiO_2 layer only needs to diffuse ~10 nm before encountering the TCO layer where it is collected. Considering that the electron transit time increases as the square of the distance, this dramatic decrease in diffusion length of 1/1000 (10 nm versus 10 microns) leads to a much faster electron transit (10^6). This allows for higher electron collection efficiencies and ultimately higher conversion efficiency. This forms the basis of our work. Here we investigate the cost-effective fabrication of the photoanodes by from AZO and TiO_2 layers.

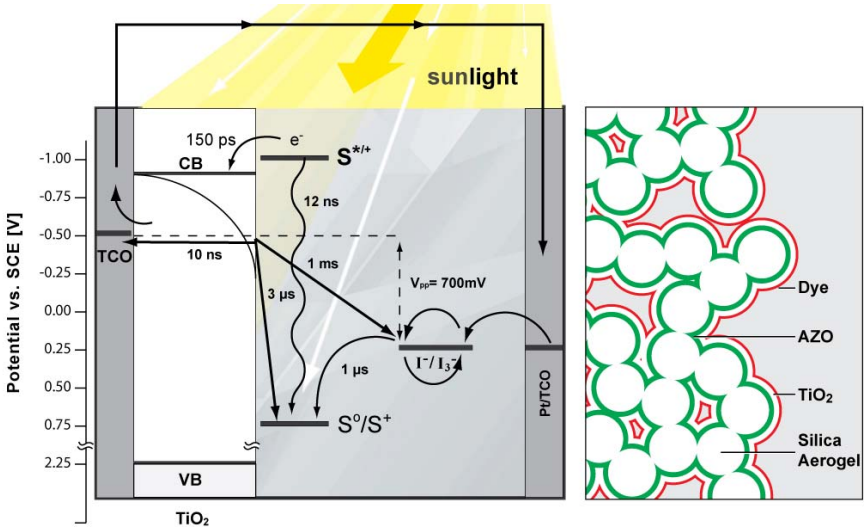

Figure 1. Competing processes in a nanostructured DSSC with significantly reduced electron transit time to conducting electrode (left); and Schematic of the nanostructured dye sensitized solar cell showing the interdigitated architecture enabled by the aerogel thin film template (right).

Experimental

The following sequence of steps was used to fabricate and evaluate our DSSCs. First silica aerogel films were deposited on fluorine-doped tin oxide (FTO) glass supports. Next, a few nanometers of titanium dioxide (TiO_2) or aluminum-doped zinc-oxide/titanium dioxide (AZO/TiO_2) layers were deposited on the silica aerogels and sensitized with dye or combination dyes. The photoanodes were assembled into photocells and their performance evaluated. A brief description of each of these processes follows.

Silica Aerogels

Silica Aerogel Formulations: A stock solution used to make the silica scaffold for the semiconducting and transparent conducting oxides is denoted herein as F-sol. The F-sol consists of monodisperse nanosilica particles, ~15 nm, synthesized at ISL, methyl cellulose X% (MCX) (Aldrich) and a very small amount of polyethylene glycol (PEG). The variation in the ratio of silica nanoparticles to MCX determines the porosity of the SiO_2 network.

Silica Nanoparticles: Silica nanoparticles were synthesized from base catalyzed (ammonium hydroxide, pH ~ 10.0) hydrolysis of tetraethylorthosilicate (TEOS) in ethanol and water adapting from the Stöber method (12). The solution was refluxed with stirring and heating at 70 °C for 16 hours, followed by cooling and two-thirds solvent removal of the ethanol by rotary evaporation. The resulting solution consisted of ~15 nm colloidal silica nanoparticles which was used as a stock solution for formulating silica aerogels. The stock solution's shelf life is six months when stored in a refrigerator.

Aqueous Polymer Solution: The aqueous polymer solution denoted as MCX, where X represents weight percent of methyl cellulose in the aqueous solution was prepared as

follows. Water was heated to 65 °C and MCX is slowly added to dissolve the polymer and prevent aggregation. After all desired MC was uniformly dissolved, the heating was stopped and the solution mixed overnight. After deaeration, the solution was ready for formulating with the colloidal silica nanoparticles and small amounts of low molecular weight PEG. These stock solutions are good for at least six months to a year.

Table 1 indicates the various stock solutions formulated using the MCX and silica nanoparticles. The thickness of the films was dictated by the ratio of silica particles to MCX and could be varied anywhere from 2 to 20 µm.

Table I. F-sol formulations used to cast silica aerogel films

Formulation	*Silica NPs*	*MCX*
Fsol2 1.1	1	1.1
Fsol2 1.5	1	1.5
Fsol2 1.5	1	1.1
Fsol2 1.5	1	1.5

After solution preparation, the aerogel thin films were deposited on FTO-coated glass substrates by the doctor blading technique to cast thick films. Two templates of varying thickness (400µm and 700µm), were used to deposit the coatings. The FTO substrate was attached to the mask using scotch tape and the solution was doctor bladed to the wells of the mask in a portable flow control booth fitted with Class 100 HEPA filters. The substrates were left to dry slowly and calcined at 470°C for one hour, with a ramp time of one hour. The nanoporous SiO_2 coated substrates were cooled at the natural rate of the furnace and shipped to our collaborators at Argonne National Laboratory (ANL) for ALD coating. Figure 2 shows the batch processing template for 40 substrates at left, and silica-coated FTO substrates at right.

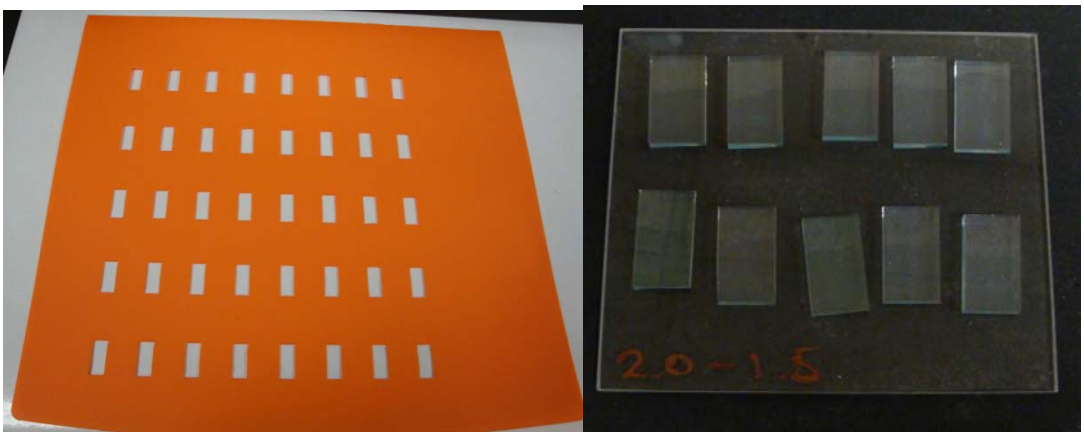

Figure 2. Template used to doctor blade 40 substrates in one batch [left]; Silica aerogel films on FTO-glass substrates (clear sections) [right].

ALD of Transparent and Semiconducting Oxide Layers

Aerogel thin films were coated in a viscous-flow hot-wall reactor under nitrogen flow at 1 Torr of pressure. A conformal coating of active layer is deposited directly onto the surface of the aerogel without collapse making this method suitable to functionalization of highly brittle surfaces. Two types of coated layers were generated. They were semiconducting (SC) TiO_2 layers directly on the silica layer, and a transparent conducting oxide (TCO) layer of aluminum-doped zinc oxide (AZO) followed by the TiO_2 layer. The ALD reactor allows the growth in substrates up to 5 cm wide in a 1 m long tube. All processes described below can be carried out in a different reactor configuration, which allows ALD on high-surface area substrates, such as 12×12 in. glass plates.

ALD of TiO_2 Thin Films: The aerogel thin films on FTO glass were coated with TiO_2 using a sequence of titanium tetrachloride and water pulses at 100 °C. Calibration of growth using flat Si and SiO_2 substrates yielded a growth rate of 0.65 Å per cycle. The samples were coated with 5, 10, 15 and 20 nm of $TiCl_4/H_2O$ at 100 °C.

ALD of Al:ZnO Thin Films: Aerogels were coated with a transparent conducting oxide layer of Al:ZnO using diethyl zinc/water pulse sequence with intercalated trimethyl aluminum/water pulses to dope the ZnO with a controlled amount of Al atoms. The ratio of Zn:Al cycles was kept 19:1. Calibration on flat substrates yielded a growth per 19:1 combined cycle of 3.3 nm.

Characterization

The coated layers were characterized by ellipsometry, scanning electron microscopy (SEM), and Raman analysis.

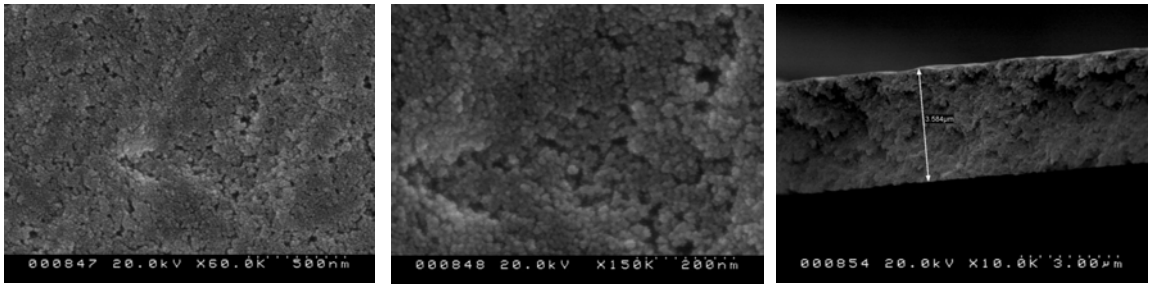

Figure 3. SiO_2 1.1 Sample with areas of moderate porosity at different magnifications [left and middle]; denser cross section of coated edge [right].

SiO_2 Films: Figure 3 illustrates a typical SiO_2 aerogel film as deposited on the surface of the FTO substrate. The silica nanoparticle size is small, 10–20 nm, in agreement with particle sizes measured by dynamic light scattering in other unpublished work performed by ISL. Depending on the template thickness and sol formulation, the silica layer thickness ranged from 20 μm to 2-3 μm in the films. A larger variation in porosity can be observed with areas of high and low porosity, as seen in Figure 3 [middle]. The SiO_2 porosity appears greater in the top view, than in the cross section [Figure 3, right], which explains later observations in ALD-TiO_2 coated SiO_2 films.

TiO_2 Films: Following ALD exposure, the coating morphology, thickness and the optical properties of the films were verified using SEM and spectroscopic ellipsometry. The SEM images in Figure 4 show the morphology of 20 nm as-deposited [left], and annealed TiO_2 coatings [right] on the surface of the aerogel. It is evident from the as-deposited TiO_2 layers that the ALD takes place homogenously on the aerogel thin film. However, due to the lower porosity on the top surface of the silica aerogel films, the subsequent ALD deposition of TiO_2 films resulted in pore clogging at the surface, and insufficient penetration of the TiO_2 layers in the interior of the aerogel scaffold. We investigated TiO_2 layers of 5, 10 and 15 and 20 nm thickness. TiO_2 layers of 20 nm thickness indicated a highly clogged surface with very little remaining porosity. Hence, we constructed photocells with photoanodes having lower TiO_2 thickness.

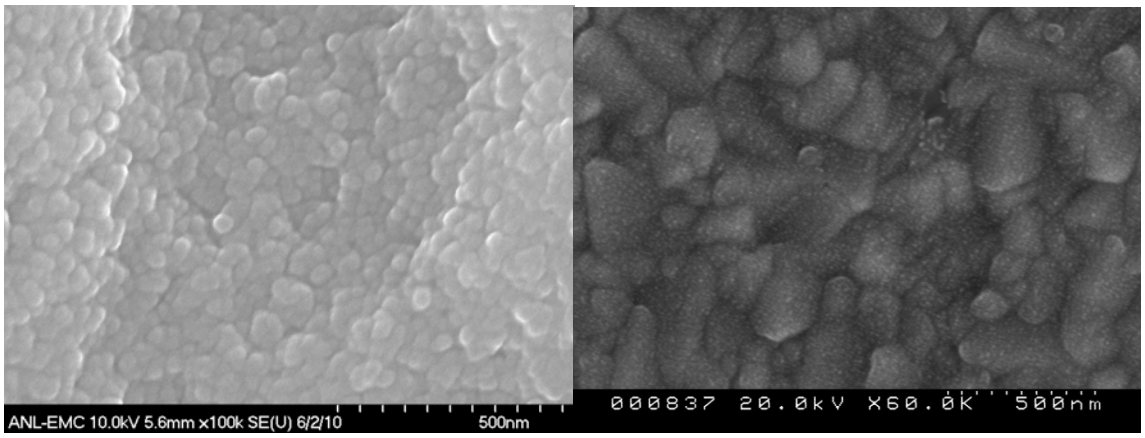

Figure 4. As deposited ALD-TiO_2 coated silica sample [left]; and after annealing at 400 ºC for 8 hours [right] showing large (100–250 nm) and small (10–20 nm) grains

As-deposited titanium dioxide coatings were amorphous and had to be annealed to form a crystal phase that could effectively transfer charge through the cell. Anatase is a suitable crystal phase with a band gap of ~ 3.2 eV. It readily accepts charge from the highest occupied molecular orbital (HOMO) of the ruthenium dye into its lowest unoccupied molecular orbital (LUMO). A post-treatment of the TiO_2-coated aerogels was carried out by annealing at 450 °C for 8 hours and cooled at a very slow rate. Alternatively, samples were annealed in N_2 at 350 °C for 15 hours, and cooled at a rate of 100 °C/hour. The anatase phase formed by annealing, is shown in Figure 4 [right]. The formation of anatase was verified by Raman spectroscopy discussed later. For the annealed TiO_2 on SiO_2 coating shown in Figure 4 [right], there was no evidence of surface porosity on the sample. The apparent grain size is in the range of 100 nm to 250 nm. In some areas the surface appears to be covered by small particles in the range of 10–20 nm indicative of possible remnants from TiO_2 coating and not that of the gold sputtered surface to enable imaging. These dense TiO_2 structures will reduce the ability for charge to efficiently transfer to the TCO underneath the TiO_2 layer of the FTO.

Ellipsometry and Raman Analysis of TiO_2 Films: The thickness and the optical properties of the films were verified using ex-situ spectroscopic ellipsometry. A multilayer model comprising the Si substrate, a 1.6 nm thick native SiO_2 layer and the TiO_2 films was used to fit the experimental data. The refractive index, n, of the TiO_2 thin films as determined by spectroscopic ellipsometry is 2.35 at 600 nm, in agreement with previous results in the literature. The influence of surface roughness on the optical

properties of the films was shown to be negligible, which suggests that flat substrates were coated homogeneously. The crystallization of the TiO_2 to anatase phase was assessed using Raman Spectroscopy. Both anatase and rutile phases of TiO_2 present signature peaks that allow an unambiguous identification of the phases. Figure 5 shows the Raman spectra for aerogel samples with 10 nm TiO_2 films grown by ALD at 100°C and after annealing at 350 °C. The Raman peaks at 396, 519 and 638 cm^{-1} for the annealed sample confirms the presence of TiO_2 in the anatase phase (11).

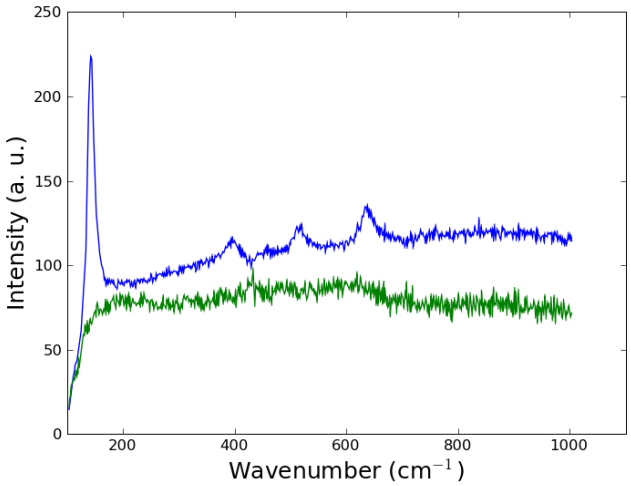

Figure 5. Raman spectra of as-deposited (no peaks) and annealed TiO_2 films (with peaks at 396, 519 and 638 cm^{-1})

AZO Films: Aerogel films on FTO glass were coated with 10 nm of Al:ZnO at 200 °C. SEM images show that Al:ZnO homogeneously coats the aerogel films. The resulting microstructure of the AZO-coated aerogels is shown in Figure 6.

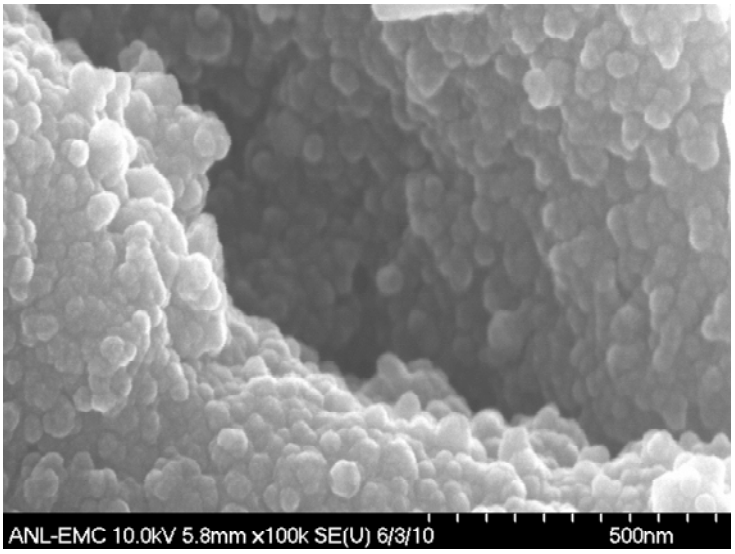

Figure 6. Scanning electron microscope image of ALD Al:ZnO coatings on silica aerogel films

The SEM images of ALD-AZO and ALD-TiO_2 layers on the aerogel coating underscore the importance of pore size and morphology in the silica scaffold to achieve a three-dimensional interpenetrating network of the semiconducting film. This is desirable to have effective and fast charge transfer from the nanoscale semiconducting film to the transparent conducting electrode. The electrical and optical properties of the 10 nm Al:ZnO layer were characterized by four-point probe measurements and spectroscopic ellipsometry. Due to enhanced electron scattering by the film-substrate and the film-air interfaces, the resistivity of the samples is higher than that of the thicker films and equal to 3×10^{-2} ohm cm. The refractive index, n, and attenuation constant, k, of the films are shown in Figure 7. According to spectroscopic ellipsometry, the k-value of the material is 0.05–0.10 for the 400–800 nm region.

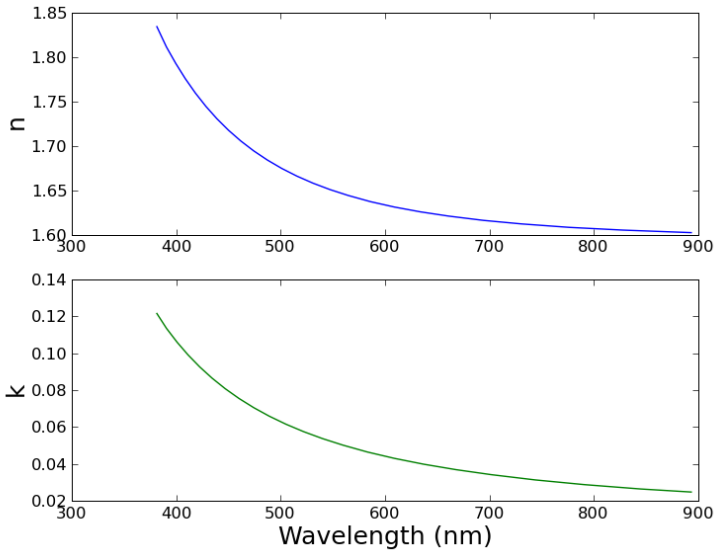

Figure 7. Optical properties of 10 nm Al:ZnO thin films deposited on aerogel/TCO glass electrodes as measured by spectroscopic ellipsometry.

The Al:ZnO coated aerogels were subsequently coated with 5 nm of TiO_2 following the procedure described previously and assembled into photocells. Once again, the denser morphology of the silica scaffold plays a large role in lowering the charge transfer efficiency from the semiconducting layers.

Dye Sensitization

Dye sensitization of the TiO_2-coated aerogel structures was accomplished by two methods. In Method A, 0.5 M of N719 was dissolved in ethanol and substrates pre-heated to 100 °C were soaked in the solution (11). We also attempted pooling 100 µL of solution to the ~0.5 in^2 coated area. After 20 hours, the substrates were rinsed with ethanol, dried in nitrogen, and used to assemble the photocells. In Method B, we used 0.02 M of the dye in 980 µL of acetonitrile and added 20 µL of tetrabutyl ammonium hydroxide (TBAOH) (13). Measured volumes (10 µL for 0.5 cm^2 TiO_2 area) of this solution was pipetted to the surface and set aside for 10 minutes. The dye-coated electrodes were rinsed with acetonitrile and used to assemble the photocells. The same method was used when co-sensitized with the Fe dye synthesized at ISL.

Fe-dye as a Co-Sensitizer: An iron-based dye was synthesized following reported procedure (14,15). A starting solution of 420.0 mg (1.72 mmol) of 2,2'-bipyridine-4,4'-dicarboxylic acid and 5 drops of 1M NaOH in 20 mL of water was heated. To this, 225.0 mg (0.575 mmol) of $Fe(NH_4)_2(SO_4)_2.6H_2O$ was added followed by dropwise addition of 1M NaOH, until complete dissolution of the ligand and subsequent formation of $[Fe^{II}$(2,2'-bipyridine-4,4'-dicarboxylic acid$)_3][SO_4]$ was indicated by a clear, dark red solution. The solution was diluted to 50 mL and heated to 90 °C. Next, 434.0 mg NaCN was added and the heating continued for 5 minutes. The pH of the cooled solution was lowered to 4.6 and the precipitated ligand was collected. The pH of the filtrate was further lowered to 2.5; the product $[Fe^{II}$-(2,2'-bipyridine-4,4'-dicarboxylic acid$)_2(CN)_2]$ was collected and rinsed with dilute H_2SO_4 and acetone. The iron dye complex was purified further by recrystallization from methanol by the addition of acetone. A black solid product was obtained at the end of the reaction sequence (265 mg) in 93.5% yield. Figure 8 shows the reaction scheme for the synthesis of the iron dye.

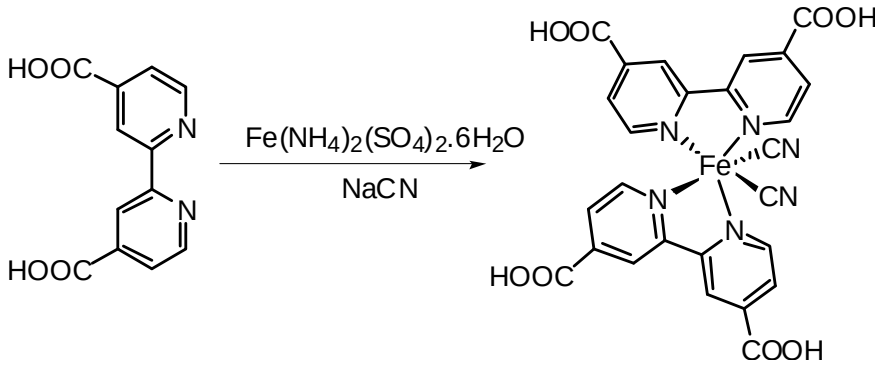

Figure 8. Reaction scheme of Fe-bipy dye synthesis

Figure 9 shows the absorbance spectra of the synthesized Fe dye. The blue dashed line represents the spectrum in dimethyl sulfoxide (DMSO) when the dye concentration is 8×10^{-5} M. The solid red line is obtained from 8×10^{-5} M solution of the dye in acetonitrile-tetrabutyl ammonium hydroxide (TBAOH) system. The bathochromic shift within the two solvent systems can be assigned to the possible ligand exchange between the cyanide and the hydroxyl anions of the TBAOH.

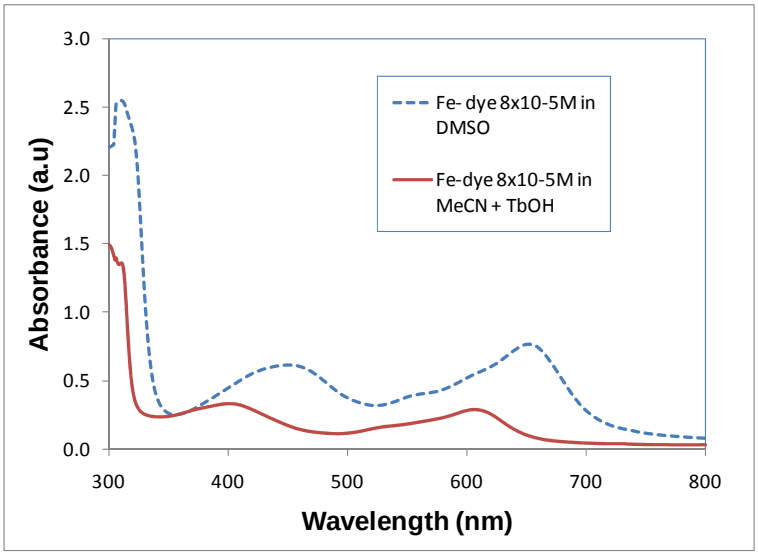

Figure 9. UV-Vis Absorbance Spectrum of Fe-dye in DMSO and in acetonitrile-TBAOH solutions

10 µL of dye solution was deposited to the surface of the TiO_2-coated samples and allowed to penetrate the porous network for 10 minutes. After the allotted soak time, excess dye was rinsed from the surface with 200 poof ethanol. Samples changed color from red (N719) to purple for the N719/Fe dye combination. It should be noted that sufficient dye uptake was not observed for samples that were not annealed. This clearly indicates that the anatase phase of TiO_2 is necessary for dye sensitization. The combination dye was delivered in a TBAOH solution consisting of 5 mM N719 and 2.5 mM Fe.

Fabrication of Photocells

The device substrates were FTO coated glass (1"×0.5"). The negative electrode (photoanode) was coated with the porous silica scaffold and then coated with the TiO_2 or AZO/TiO_2 layers. The photoanodes were sensitized with the dye as described earlier. The positive or counter electrode was platinized in the following manner. Briefly, a 1 mm hole was drilled into the FTO substrates prior to cleaning. Then substrates were cleaned in common degreasing and cleaning solvents and dried. A drop of 5 mM chloroplatinic acid in isopropanol was cast onto the FTO surface and left to dry for 5 minutes in a draft-free hood, and heat treated at 385 °C for 20 minutes to form the platinized electrodes.

Electrical leads were connected to the active FTO layer on each electrode with conductive silver epoxy. Photocells were then constructed by clamping the platinized electrode to the sensitized titania-coated electrode. Between these two electrodes, a 0.25 mm thick Surlyn^{TM} spacer was used to create separation for the electrolyte. Two electrolytes were investigated. Electrolyte A consisted of 0.6 M butylimmidazolium iodide, 0.03 M Iodine, 0.1 M guanadinium thiocyanate and 0.5 M 4-tert-butylpyridine in acetonitrile/valeronitrile, (85/15). Electrolyte B contained 0.5 M lithium iodide, 0.05 mM I2, 0.5 M t-butyl pyridine, and 3-methoxypropionitrile. Screening tests using a Gratzel cell configuration showed that Electrolyte A offered better charge transfer and performance than Electrolyte B.

Testing of Photocells

The potential-current (I-V) curve of assembled photocells was recorded using a Princeton Applied Research Potentiostat/Galvanostat Model 263A. The samples were irradiated with simulated solar energy supplied by a Newport 150 W Solar Simulator Model 96000 fitted with a 1.5 A.M. filter and a beam turner. The test setup for evaluating solar cells is shown in Figure 10.

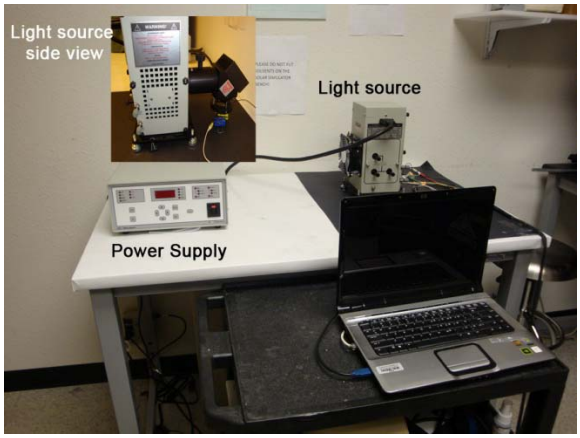

Figure 10. Test setup showing 150 Watt solar simulator fitted with beam turner and AM 1.5 global filter.

Discussion

To calculate the efficiency of the dye sensitized solar cells, the fill factor, FF, was determined from the following equation (16):

$$FF = \frac{j_{mp} \times V_{mp}}{j_{sc} \times V_{oc}} \qquad [1]$$

Practically, the fill factor, FF, is the ratio of the area bound by the current density at maximum power (j_{mp}) and the voltage at maximum power (V_{mp}), and the area bound by the short circuit current density (j_{sc}) and the open circuit voltage (V_{oc}). As an example, we obtained a fill factor of ~36% or a Gratzel-type cell made from nanoparticle TiO_2 powders.

The efficiency, η, of a solar cell is defined by (16):

$$\eta = \frac{FF \times j_{sc} \times V_{oc}}{I_{inc}} \times 100 \qquad [2]$$

where the efficiency is dependent upon the short circuit current density, j_{sc} (mA/cm^2), the open circuit voltage (V_{oc}), the fill factor, and the intensity of the incident light, I_{inc} (mW/cm^2).

The Gratzel-type cell tested here offered an efficiency of <1%. One way to improve upon the efficiency is to change the dye to a system that absorbs more light. We investigated using the Fe dye to improve upon these characteristics. The Fe dye exhibited better photon absorption characteristics, but did not offer desirable photocell performance when used independently. However, by mixing the Fe dye with N719 dye, we found that the performance of the system improved greatly compared to using the N719 dye alone.

The calculated efficiency of the Gratzel-type cells constructed with the N719/Fe combination dye in Electrolyte A is approximately 2.2%. The fill factor for these samples is approximately 41.2%. A comparison of the two fill factors is presented in Figure 11 (right).

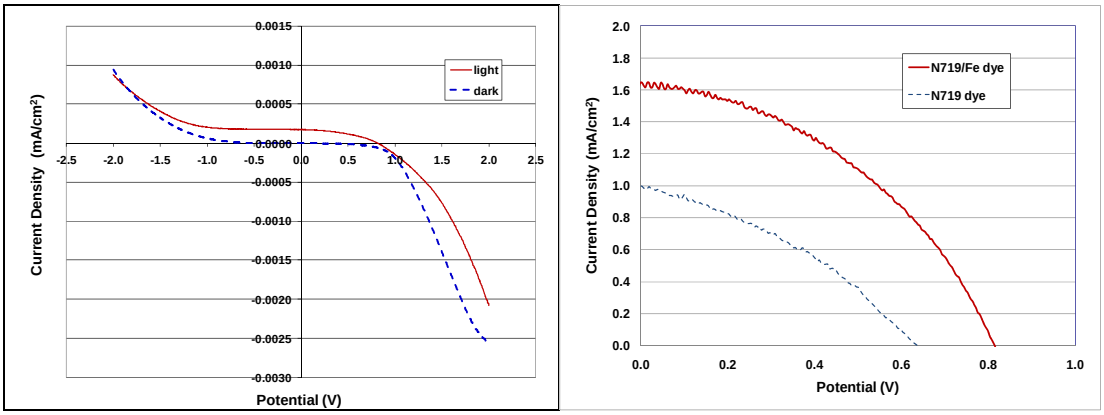

Figure 11. I-V Curve for N719/Fe dye combination in Gratzel-type cell with Electrolyte A at 10% Sun (left); Comparing Fill Factor of N719/Fe combination dye and N-719 in Electrolyte A at 10% Sun (right).

It is apparent that the addition of the Fe dye greatly increases the fill factor of the Gratzel-type cell. We also constructed photovoltaic devices based on coated aerogel scaffolds that were sensitized with the N719 dye. It was found that using the Gratzel cell-type arrangement consisting of nanoporous titanium dioxide structure, a 2:1 molar ratio of the Ru:Fe dye sensitizers, improved the overall device efficiency from 0.87% to 2.2%. The same effects were observed for the aerogel structured devices, in which the efficiency increased from 0.10% to 0.27%. More work is ongoing to optimize the aerogel scaffold and characterize the ALD-coated aerogel photoanodes and assembled photocells.

Conclusions

It was not the purpose of this work to compare efficiencies with reported values. Instead, the focus was to establish the potential by showing tangible improvements during the short term duration of the project. The next phase would allow us to demonstrate the true potential of our approach via efficiency comparison with the state of the art DSSC cell. The lower efficiencies for the photocells suggest that the charge transfer from the dye to the semiconducting layer and subsequent transport to the FTO electrode must be significantly improved. An explanation for the low efficiencies can be derived from the SEM morphology of the silica and subsequent ALD-coated TiO_2 or ALD-AZO-TiO_2 layers. The SEM images indicate a denser top surface in the silica coatings, which leads to pore clogging when coated by ALD-TiO_2 layers. This indicates that the silica aerogel structure must be optimized to produce voids ~ 100 nm in diameter, significantly larger than the 30-40 nm voids observed in the SEM. A similar observation was made for the AZO layers. Here too, pores of the aerogel were clogged by ALD

deposition of AZO and TiO_2, leading to little or no contact with the FTO electrode. Therefore, electron transfer from the TiO_2 layer to the FTO electrode was poor. TiO_2–coated aerogels (10 nm) exhibited small regions where TiO_2 layers percolated to the FTO electrode leading to low performance. Optimizing the pore structure and morphology in the aerogel scaffold would be key to achieving the interpenetrating architecture of the transparent conducting oxide layer, which in turn can promote fast electron transfer and consequently increase photocell efficiency.

Acknowledgments

This work was carried out through funding from the Department of Energy Grant # DE-SC0003370.

References

1. N.S. Lewis, *Report on the Basic Energy Sciences Workshop on Solar Energy Utilization.* U.S. Department of Energy, Office of Science (2005).
2. D. Gwinner and A. Hicks, *Our solar power future: The U.S. photovoltaics industry roadmap through 2030 and beyond*. U.S. Department of Energy, Office of Energy Efficiency and Renewable Energy (2004).
3. V.M. Fthenakis, H.C. Kim, and E.A. Alsema, *Environmental Science and Technology*, **42,** 2168 (2008).
4. E.A. Alsema, *Prog. Photovolt: Res. Appl*., **8**, 17 (2000).
5. H.A. Aulich and F. Schulze, *Prog. Photovolt: Res. Appl.*, 2002. **10**: p. 141-147.
6. E.A. Alsema and M.J. DeWild-Scholten, *Life-Cycle Analysis Tools for Green Materials and Process Selection*, **895**, 73 (2006).
7. M. Gratzel, *Journal of Photochemistry and Photobiology C: Photochemistry Reviews*, **4**, 145 (2003).
8. M. Gratzel, *Chemistry Letters*, **34**, 8 (2005).
9. A.B.F. Martinson, J.W. Elam, J.T. Hupp, and M.J. Pellin, *Nano Letters*, **7**, 2183 (2007).
10. T.W. Hamann, A.B.F. Martinson, J.W. Elam, M.J. Pellin and J.T. Hupp, *Adv. Mater.,* **20**, 1560 (2008).
11. T.W. Hamann, A.B.F. Martinson, J.W. Elam, M.J. Pellin and J.T. Hupp, *J. Phys. Chem. C.,* **112**, 10303 (2008).
12. W.A. Stöber, A. Fink, and E. Bonn, *J. Colloid. Interface. Sci*., **26**, 62 (1968).
13. M.K. Nazeeruddin, R. Splivalio, P. Lisko, P. Comte and M. Gratzel, *Chem. Commun*., 1456 (2003).
14. S.K. Deb, R. Ellington, S. Ferrere, A.J. Frank, B.A. Gregg, A.Z. Nozik, N. Park and G. Schlichthörl, NREL/CP-590-25056 *In 2nd Word Conference on Photovoltaic Solar Energy Conversion*; Vienna, Austria, (1998).
15. A.A. Schilt, *J. Am. Chem. Soc*., **82,** 3000 (1960).
16. M. Gratzel, *Accounts in Chemical Research*, **42**, 1788 (2009).